ADVANCED ENERGY MATERIALS
www.advenergymat.de

Light-Driven $BiVO_4$–C Fuel Cell with Simultaneous Production of H_2O_2

*Xinjian Shi, Yirui Zhang, Samira Siahrostami, and Xiaolin Zheng**

Photoelectrochemical (PEC) systems have been researched for decades due to their great promise to convert sunlight to fuels. The majority of the research on PEC has been using light to split water to hydrogen and oxygen, and its performance is limited by the need of additional bias. Another research direction on PEC using light, is to decompose organic materials while producing electricity. In this work, the authors report a new type of unassisted PEC system that uses light, water and oxygen to simultaneously produce electricity and hydrogen peroxide (H_2O_2) on both the photoanode and cathode, which is essentially a light-driven fuel cell with H_2O_2 as the main product at the two electrodes, meanwhile achieving a maximum power density of 0.194 mW cm^{-2}, an open circuit voltage of 0.61 V, and a short circuit current density of 1.09 mA cm^{-2}. The electricity output can be further used as a sign for cell function when accompanied by a detector such as a light-emitting diode (LED) light or a multimeter. This is the first work that shows H_2O_2 two-side generation with a strict key factors study of the system, with a clear demonstration of electricity output ability using low-cost earth abundant materials on both sides, which represents an exciting new direction for PEC systems.

1. Introduction

Photo-electrochemical (PEC) water splitting system has been investigated over four decades following the seminal discovery by Fujishima and Honda in 1972.[1] Majority research on PEC has been focusing on using light to split water to hydrogen and oxygen, which frequently requires additional input of electrical energy.[2] However, broadly speaking, a PEC system means that photoelectrodes absorb light to generate charge carriers to react with electrolytes, a definition that implies much broader applications than just water splitting. For example, photogenerated holes can be used to degrade hazardous organics for waste water treatment,[3] and photogenerated electrons can be used for other thermodynamically favorable reactions beyond hydrogen evolution, such as O_2 reduction reaction. Thus, a PEC system can operate under moderate bias or even without bias to produce electricity.[4,5] Such an unassisted PEC system was first referred as photocatalytic fuel cells (PFCs) in 2006,[6] for which the photoanode oxidizes NH_3 to N_2 or decomposes various biomass, and cathode reduces O_2 to H_2O. This PFC system also produces electricity. To date, all the PFC-related works have been focusing on organics degradation on photoanodes.[3,4,7] It will be valuable to create a new type of unassisted PEC system that simultaneously produces valuable chemicals like PEC water splitting cells and electricity as PFC cells.

In this work, we report such an unassisted PEC system that uses light, water, and oxygen to simultaneously produce electricity and hydrogen peroxide (H_2O_2) on both photoanode ($BiVO_4$) and cathode (carbon), i.e., light + $2H_2O$ + O_2 = electricity + $2H_2O_2$. There have been several reports on unassisted H_2O_2 generation from one side or two sides.[8,9] However, the two-side generation has its specialty and needs to be considered on the compatibility between electrode materials, electrolytes, and any cross talk between two sides, to promote the H_2O_2 generation efficiency to a maximum. So far, no such work has been done regarding the two-side H_2O_2 generation as an individual case with the key factors' studies for the systematical level optimization rather than simple combination of two single-side generations. As a result, for this work, the optimized unassisted PEC system produces H_2O_2 at a rate of 0.48 μmol min^{-1} cm^{-2} and a maximum output power density of 0.194 mW cm^{-2} (0.61 V open-circuit potential and 1.09 mA cm^{-2} short-circuit current density). In essence, this unassisted PEC system is a light-driven fuel cell with H_2O_2 as the main product on both electrodes. The electricity output can be also used for a signal of cell function, when it is accompanied by a detector such as a light-emitting diode (LED) light or a multimeter, as shown in the end of this work.

In the following sections, we will first discuss the design of this light-driven fuel cell, followed by the optimization

X. Shi, Y. Zhang, Prof. X. Zheng
Department of Mechanical Engineering
Stanford University
Stanford, CA 94305, USA
E-mail: xlzheng@stanford.edu
Y. Zhang
Department of Mechanical Engineering
Massachusetts Institute of Technology
MA 02139, USA
Dr. S. Siahrostami
SUNCAT Center for Interface Science and Catalysis
Department of Chemical Engineering
Stanford University
443 Via Ortega, Stanford, CA 94305, USA
The ORCID identification number(s) for the author(s) of this article can be found under https://doi.org/10.1002/aenm.201801158.

DOI: 10.1002/aenm.201801158

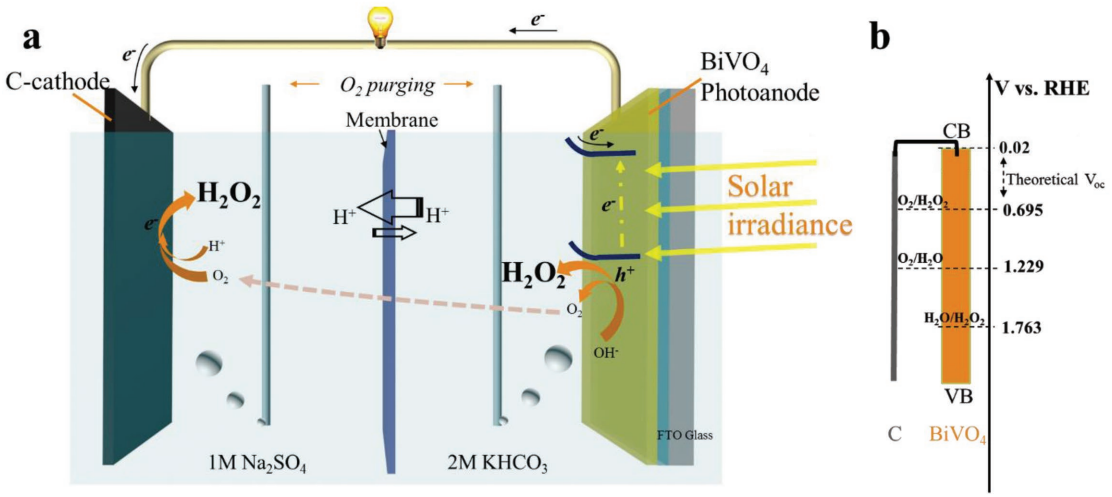

Figure 1. a) Schematic illustration of the design of light-driven fuel cell with spontaneous H_2O_2 generation. The light bulb illustrates the simultaneous produced electricity that flow through the external circuit (Movie S1 and Figure S9, Supporting Information). b) The band diagram of the system. The conduction band (CB) and valence band (VB) edge positions of $BiVO_4$ straddle the redox potentials of O_2/H_2O_2 and H_2O/H_2O_2, suggesting the possibility of unassisted H_2O_2 production. The theoretical V_{oc} for the light-driven fuel cell is 0.693 V, estimated from the CB of $BiVO_4$ and O_2/H_2O_2 redox potential (main text Section 1).

procedures to maximize H_2O_2 production, and characterization of the fuel cell performance.

2. Results and Discussion

2.1. Thermodynamic Analysis and Design of the Light-Driven Fuel Cell

Figure 1a schematically illustrates the design of the light-driven fuel cell for producing electricity and H_2O_2 on both electrodes. To produce H_2O_2 while using only water and oxygen as reactants, photoanode needs to evolve water oxidation reaction (WOR, reaction (1)) and cathode needs to advance oxygen reduction reaction (ORR, reaction (2)). Both WOR and ORR are two-electron pathways and they are expressed below for the acidic condition, where E° is cited from the standard potentials in aqueous solution[10]

$$\text{Anode}: 2H_2O \leftrightarrow H_2O_2 + 2(H^+ + e^-), \quad E^\circ_{ox} = -1.763\ \text{V} \tag{R1}$$

$$\text{Cathode}: O_2 + 2(H^+ + e^-) \leftrightarrow H_2O_2, \quad E^\circ_{red} = 0.695\ \text{V} \tag{R2}$$

$$\text{Overall reaction}: 2H_2O(l) + O_2 = 2H_2O_2, \quad \Delta E_{cell} = -1.068\ \text{V} \tag{R3}$$

Note that the negative sign in reaction (1) has no strict thermodynamical significance, which is merely used for the calculation to get reaction (3) to show that the cell under dark condition is not self-driven (Figure S1 and Supplementary Note S1.1, Supporting Information). However, in a PEC system, we can choose semiconductor electrodes to generate photocarriers with enough energy to drive reactions (1) and (2). For example, the n-type semiconductor $BiVO_4$ (Figure 1b) has a conduction band (CB) edge around 0.02 V versus reversible hydrogen electrode (RHE) based on the measurement in electrolyte,[11] which is more negative than the redox potential for O_2/H_2O_2 (0.695 V vs RHE). Since $BiVO_4$ has a bandgap ≈2.4 eV, its valance band (VB) edge is more positive than the redox potential for H_2O/H_2O_2 (1.763 V vs RHE). Thermodynamically, the band positions of $BiVO_4$ allow production of H_2O_2 through both reactions (1) and (2) under illumination without additional bias (Figure 1b). Such a system works as a light-driven fuel cell with a theoretical open-circuit voltage of 0.693 V, determined by the difference between the redox potential of O_2/H_2O_2 and the CB edge of $BiVO_4$ (=0.695–0.02 V). We have also estimated that the maximum H_2O_2 generation rate on $BiVO_4$ is ≈4.6 μmol min^{-1} cm^{-2} under 1 sun 1.5G AM solar spectrum assuming a full light absorption of $BiVO_4$ above 2.4 eV and all the photogenerated charge carriers are used for H_2O_2 production (Figure S2 and Supplementary Note S1.2, Supporting Information).

2.2. Components Optimization for H_2O_2 Production on Both Photoanode and Cathode

The analysis above shows the feasibility for such a light-driven fuel cell system with simultaneous H_2O_2 production on both electrodes. Next, we discuss the optimization of each component of the entire light-driven fuel cell while prioritizing the H_2O_2 production over electricity generation. A general fuel cell has four key components, i.e., electrodes separated by a membrane, electrolyte, reactants on each electrode, and output products. We will discuss our selection of each of these components for this specific light-driven fuel cell.

2.2.1. Selection of Materials for Photoanode and Cathode

In Section 1, we have briefly mentioned the electrode material used for the feasibility analysis of this light-driven fuel cell. Below, we will discuss the rationality for selecting $BiVO_4$ as the photoanode and carbon as the cathode. The material selection criteria of the electrode include its activity (i.e., current density), its selectivity toward H_2O_2 (i.e., Faraday efficiency FE), its stability and potential cost, and the impact of electrode materials on the stability of H_2O_2. Among those criteria, the first priority is the selectivity as other reactions can occur on both anode and cathode to compete over H_2O_2 production. At photoanode, the H_2O_2 generation reaction (reaction (1)) competes with two other WOR reactions. One is the four-electron pathway for O_2 evolution reaction (reaction (4)), which occurs at a lower potential. The other is the one-electron pathway for OH radical generation (reaction (5)), which occurs at a higher potential.[12]

$$2H_2O \leftrightarrow O_2 + 4(H^+ + e^-), \quad E^\circ = 1.229\ \text{V} \tag{R4}$$

$$H_2O \leftrightarrow OH^{\bullet}(aq) + (H^+ + e^-), \quad E^\circ = 2.38\ \text{V} \tag{R5}$$

The selectivity of H_2O_2 production from electrochemical WOR (reaction (1)) has been experimentally investigated over several metal oxides MnO_x,[13] $BiVO_4$,[14,15] SnO_2,[16] WO_3,[14,15] and TiO_2.[14] These studies have identified $BiVO_4$ as a top anode choice due to its high Faraday efficiency for H_2O_2 production. Our recent theoretical and experimental studies further showed that $BiVO_4$ has a high selectivity toward H_2O_2 production over reactions (4) and (5) when the applied bias is moderate (2.9–3.3 V vs RHE) under dark and lower (1.5–2.3 V) under 1 sun illumination.[15] Finally, the CB and VB edge positions of $BiVO_4$ straddle the redox potentials of reactions (1) and (2) (Figure 1b), suggesting the possibility of unassisted H_2O_2 production. Hence, we chose $BiVO_4$ as the photoanode for H_2O_2 production under illumination. Herein, $BiVO_4$ film was made on fluorine-doped tin oxide (FTO) substrate with a sol–gel process (see the Experimental Section).

At cathode, the H_2O_2 generation reaction from ORR (reaction (2) competes with the following four-electron pathway reaction, which produces H_2O instead of H_2O_2

$$O_2 + 4(H^+ + e^-) \leftrightarrow 2H_2O, \quad E^\circ = 1.229\ \text{V} \tag{R6}$$

Reaction(2) also competes with hydrogen evolution reaction (HER), which is thermodynamically more favorable in a high acidic medium at lower biases.

$$2H^+ + 2e^- \leftrightarrow H_2, \quad E^\circ = 0\ \text{V} \tag{R7}$$

There are many options for cathode materials. Pt–Hg and Pd–Hg are the best catalytic materials for two-electron ORR toward H_2O_2 with high activity and selectivity.[17] Many other catalysts, such as Au,[9] PdAu alloy,[18] cobalt porphyrin,[8,19] carbon-based materials,[20] and even commercial carbon[21] have also exhibited reasonable selectivity toward H_2O_2 generation. Considering the selectivity and potential scalability, we chose carbon supported on carbon paper as the cathode, hereinafter referred to as C-cathode. To make the C-cathode in this work, the ordered mesoporous carbon powder was dispersed in solvent and further drop casted to the Sigracet Graphite carbon paper (see the Experimental Section). Both electrodes were tested under the three-electrode system with Ag/AgCl as the reference electrode. When we compare our C-cathode with Au film and bare C paper, the C-cathode shows superior ORR performance toward H_2O_2 production regarding both the onset potential and level of current density (Figure S1b, Supporting Information). Supplementary Note S1.3 (Supporting Information) discusses more information on the photoanode and cathode selection and optimization.

2.2.2. Electrolyte Selection for Photoanode and Cathode Sides

Similar to typical fuel cells, two-chamber setup has been applied previously and is critical to avoid H_2O_2 generated on the cathode from being disproportionated on the anode. In this work, we utilize the setup and further improve upon it by optimizing the electrolyte in each chamber for enhanced H_2O_2 production. Here, we tested the effect of two common electrolytes, i.e., sulfate (Na_2SO_4) and bicarbonate ($KHCO_3$), on the H_2O_2 production over the $BiVO_4$ photoanode and the C-cathode, respectively. For each electrode, we used it as the working electrode in a three-electrode system, with Ag/AgCl as the reference electrode and FTO as the counter electrode. For the C-cathode, we used the O_2-saturated condition.

The $BiVO_4$ photoanode was tested under 1 sun illumination. As shown in **Figure 2**a,c, using $KHCO_3$ leads to both higher FE for H_2O_2 generation and higher H_2O_2 generation rate (0.6 V vs RHE) than using Na_2SO_4. In addition, the onset potential for photocurrent is lower for $KHCO_3$ than Na_2SO_4 (Figure S3a, Supporting Information). All these results show that $KHCO_3$ is a better electrolyte than Na_2SO_4 for H_2O_2 production. Based on previous studies,[14,22] one possibility is that the HCO_3^- anion acts as a catalyst for H_2O_2 production. HCO_3^- is oxidized by photogenerated holes to HCO_4^- (reaction (8)), which further oxidizes H_2O to H_2O_2 forming HCO_3^- (reaction (9)).[23]

$$HCO_3^- + H_2O \leftrightarrow HCO_4^- + 2(H^+ + e^-) \tag{R8}$$

$$HCO_4^- + H_2O \leftrightarrow H_2O_2 + HCO_3^- \tag{R9}$$

Here HCO_4^- is not just a conveniently conjured up species, but it is actually a real peroxide with the structure $HOOCO_2^-$, as evidenced by the NMR and other vibrational spectroscopy measurements[23] with some other studies.[23] Thus, the presence of HCO_3^- facilitates two-electron pathway toward forming H_2O_2 for photoanode. In addition, when using $KHCO_3$, the FE for H_2O_2 production achieves a peak value of 95% at 1.7 V versus RHE (Figure 2a). The FE for H_2O_2 is smaller at lower bias due to the competition of O_2 production (reaction (4)). The FE for H_2O_2 is smaller at higher bias due to the competition of $OH^{\bullet}$ generation (reaction (5)).

The case is more interesting and remarkable for the cathode part. Figure 2b shows that the FE for H_2O_2 production

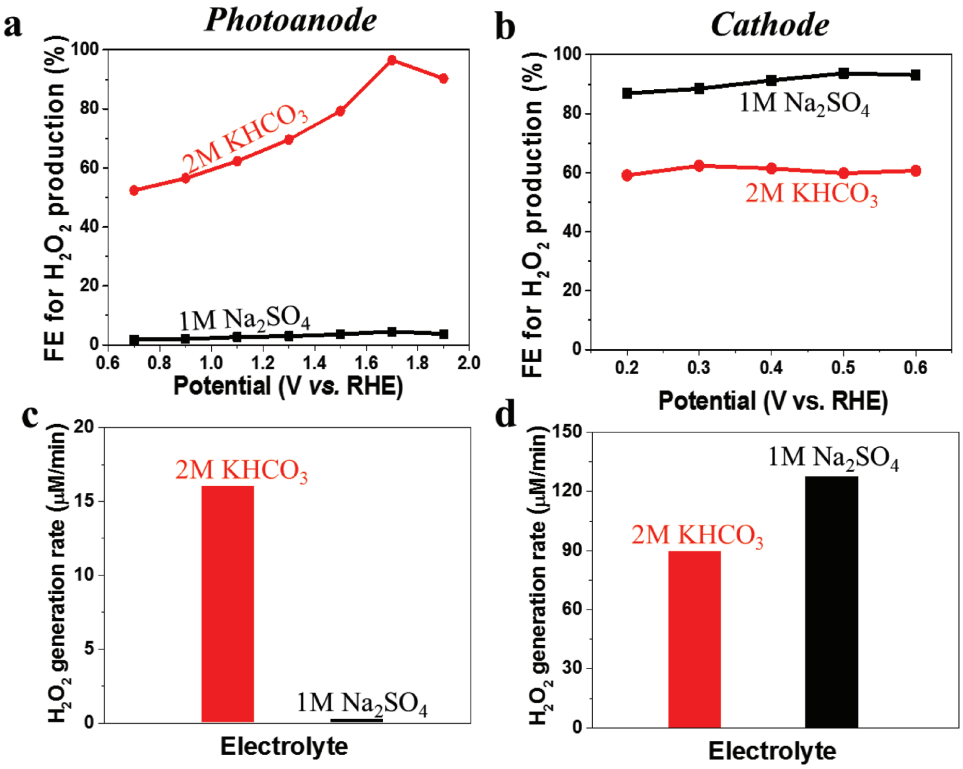

Figure 2. Effects of electrolyte on the H_2O_2 production on $BiVO_4$ photoanode and C-cathode, respectively. Faraday efficiencies for H_2O_2 production vs. applied potential for a) $BiVO_4$ photoanode under 1 sun illumination and b) C-cathode. The H_2O_2 generation rates at 0.6 V versus RHE for c) $BiVO_4$ photoanode under 1 sun illumination and d) C-cathode. The results indicate that $KHCO_3$ is a better electrolyte for $BiVO_4$ photoanode and Na_2SO_4 is a better electrolyte for C-cathode. All the tests were conducted in a three-electrode system with the tested electrode as working electrode, Ag/AgCl as reference electrode, and bare FTO as counter electrode. All the electrolytes were O_2 saturated with a pH of 8.3 during tests.

in $KHCO_3$ is about 20% lower than that in Na_2SO_4 at the C-cathode. The H_2O_2 generation rate at 0.6 V versus RHE is also higher for Na_2SO_4 than $KHCO_3$ (Figure 2d). Cathode is different with the photoanode because it has abundant electrons, which promotes reaction (8) to proceed in the reverse direction. The resulting higher concentration of HCO_3^- consumes H_2O_2 through the reverse reaction of reaction (9), leading to lower H_2O_2 production with $KHCO_3$ (Figure S4, Supporting Information). Although the benefit of bicarbonate electrolyte to two-electron pathway water oxidation has been generally reported, in this work, it is the first time to notice its negative effect to H_2O_2 production when under reduced condition.

In addition, unlike photoanode, the FE for H_2O_2 production on the C-cathode is not very sensitive to the applied bias (Figure 2b). The $KHCO_3/Na_2SO_4$ also sets the system in a favorable pH range for H_2O_2 production. More details on the electrolyte species selection and pH effect for the cathode part are provided in Supplementary Note S1.4 and Figure S3b (Supporting Information).

2.2.3. Effect of O_2 Purging on H_2O_2 Production at Both Electrodes

O_2 is a reactant to form H_2O_2 (reaction (1)) at cathode, but it is an undesired product for oxygen evolution reaction (reaction (4)) at photoanode. If no additional O_2 is provided to the cathode, cathode has to use the initial O_2 dissolved in the electrolyte and the produced O_2 from the photoanode. The consumption of O_2 in reaction (1) will drive reaction (4) move in the forward direction, resulting in less H_2O_2 production on photoanode. Such limited source of O_2 and cross talk between two electrodes[24] will impact the H_2O_2 production at both electrodes. This implies that O_2 should be provided on both electrodes to facilitate H_2O_2 production.

To confirm the importance of O_2 purging, we compared the amount of H_2O_2 production on both photoanode and cathode with and without O_2 purging. Experiments were carried out separately for $BiVO_4$ and C-cathode as the working electrode in a three-electrode system. For the $BiVO_4$ photoanode, a constant bias of 0.6 V versus RHE is applied together with 1 sun illumination, while C-cathode is used as the counter electrode to allow O_2 reduction to H_2O_2 at the counter and Ag/AgCl as the reference electrode. The electrolyte used for the working electrode is 2 M $KHCO_3$ and for the counter electrode is 1 M Na_2SO_4, and they are separated with a membrane as optimized above. **Figure 3**a plots the H_2O_2 concentration at the photoanode with/without O_2 purging as a function of time. For the first 4 min of testing, the electrolyte is not mechanically stirred, so the O_2 diffusion between two electrodes is slow. As such, the O_2 purging has little impact on the H_2O_2 production at the $BiVO_4$ photoanode since it neither needs O_2 as a reactant nor provides much O_2 to the cathode. At $t = 4$ min, mechanical stirring is introduced to both half-cells to accelerate O_2 transport in between. Under the fast O_2 transport condition, the H_2O_2

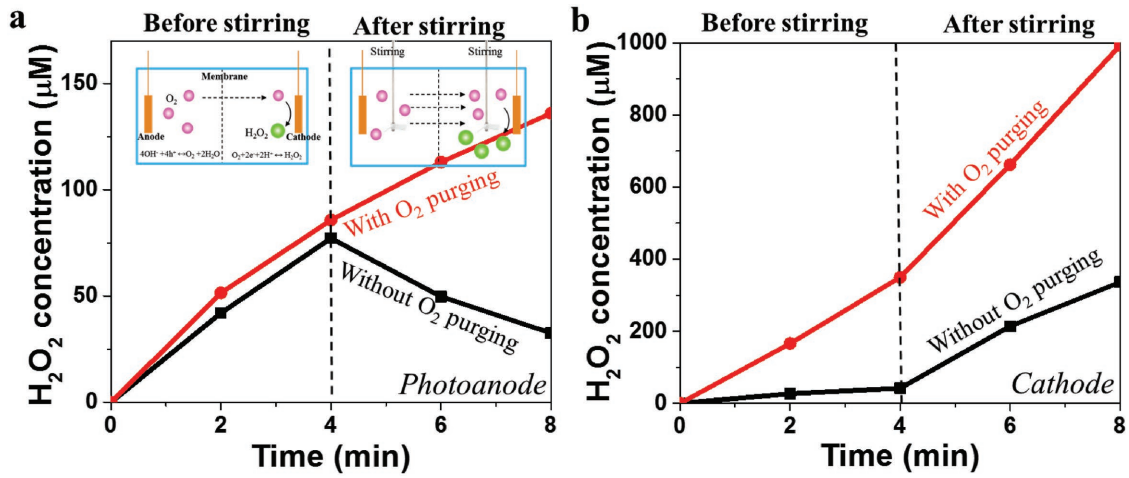

Figure 3. Effects of O_2 purging on the H_2O_2 production on $BiVO_4$ photoanode and C-cathode, respectively. The H_2O_2 concentration versus time for a) $BiVO_4$ photoanode under 1 sun illumination and b) C-cathode with and without O_2 purging. For the first 4 min, no stirring is applied and O_2 diffuses slowly between electrodes. From $t = 4$ min, stirring is applied to promote O_2 exchange between two electrodes. The results show that O_2 purging is necessary to promote H_2O_2 production on both electrodes.

concentration at the photoanode continues to increase with O_2 purging but starts to drop without O_2 purging. The reason is that under stirring and without O_2 purging, O_2 produced at the photoanode is fed to cathode and consumed there. This not only perturbs the competition between reaction (1) for H_2O_2 production and reaction (4) for O_2 production but also promotes the consumption of H_2O_2 to form O_2. The combination of slower production and faster consumption leads to the reduction of H_2O_2 concentration. The H_2O_2 concentration will not continuously go down but rather eventually stabilizes or increases in a much slower rate when the generation and consumption for H_2O_2 reach balance, as evidenced by a 20 min measurement in Supplementary Note S2 (Supporting Information).

The similar process is used to study the effect of O_2 purging on the H_2O_2 production on the C-cathode as the working electrode under a constant applied bias of 0.6 V versus RHE, while $BiVO_4$ is used as the counter electrode and Ag/AgCl as the reference electrode. Figure 3b plots the H_2O_2 concentration at the cathode as a function of time with/without O_2 purging. Regardless of the stirring, O_2 purging increases the H_2O_2 production at the C-cathode since it is the reactant for H_2O_2 production. When the mechanical stirring starts at $t = 4$ min, the production rate increase of H_2O_2 (slopes in Figure 2b) is more pronounced for the case without O_2 purging than that with O_2 purging. More quantitative analysis on the O_2 purging effect under a two-electrode system is discussed in Supplementary Note S2 and Figure S5 (Supporting Information).

2.2.4. Simultaneous H_2O_2 PEC Production on Both $BiVO_4$ Photoanode and C-Cathode

The results above identify the optimal conditions for the two-electrode PEC production of H_2O_2 as follows—photoanode: $BiVO_4$ with 2 M $KHCO_3$ (15 mL) as electrolyte, cathode: C-cathode with 1 M Na_2SO_4 (10 mL) as electrolyte, with a membrane in between and O_2 purging on both sides. With these conditions, an external bias of 1.5 V is applied between the two electrodes and the photoanode is under 1 sun illumination from the back side. The H_2O_2 concentrations on both electrodes are plotted as a function of time in **Figure 4**a. The concentration of H_2O_2 reaches ≈2610 ppm (≈0.26 wt%) at the cathode and 1530 ppm at the anode after 300 min of test. The concentration of the produced H_2O_2 here is high enough for applications such as inhibition of endogenous peroxidase in immunohistochemistry.[25] We calculated the normalized H_2O_2 generation rate per geometrical area of electrode (Supplementary Note S1.5, Supporting Information) to compare the performance of our system with other PEC systems for H_2O_2 production. The normalized H_2O_2 production rate under 1.5 V per unit time and per geometric area of our system is 2.42 μmol min^{-1} cm^{-2}, which is much higher than other electrochemical systems for H_2O_2 production with even higher applied bias with or without illumination (**Table 1**).

Besides, we tested the potential of our two-electrode system to produce H_2O_2 using tap water and distilled water. Figure 4b shows that the concentration of H_2O_2 reaches 420 ppm/cathode and 67 ppm/photoanode with tap water, while 280 ppm/cathode and 39 ppm/photoanode with distilled water. It should be noted that the concentration of H_2O_2 here already reaches the level for the commercial water disinfectant (D-50/500 (bafry), 35 ppm for treating drinking water[26]), for which the main component is H_2O_2.

2.3. Characterization of the Light-Driven Fuel Cell for H_2O_2 and Electricity Generation

Figure 5a is the *J–V* curve for our two-electrode system under 1 sun illumination which shows a notable current flow (1.09 mA cm^{-2}) without external bias. Figure 5b also illustrates that the *J–V* curves of WOR and ORR intersect at 0.66 V versus RHE. These results confirm our discussion above that this system can be used to generate H_2O_2 without additional bias. To confirm this, Figure 5c shows the chopped current density–time (*J–t*) curve under 1 sun illumination without external bias. Under this

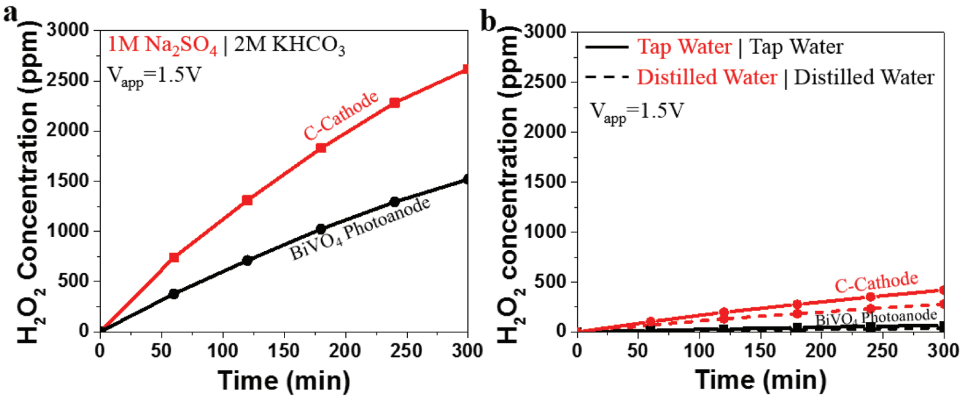

Figure 4. Production rates of H_2O_2 on $BiVO_4$ photoanode (under 1 sun illumination from the back side) and C-cathode in a two-electrode system with O_2 purging on both sides with an applied bias of 1.5 V. a) Using the optimized electrolytes (15 mL 2 M $KHCO_3$ at the anode part, 10 mL 1 M Na_2SO_4 at the cathode part). b) Using tap water (solid lines) and distilled water (dashed lines) as electrolytes for both electrodes.

condition, the total H_2O_2 generation rate is 0.18 µmol min^{-1} cm^{-2} (FE = 53%) for photoanode and 0.30 µmol min^{-1} cm^{-2} (FE = 92%) for cathode. The sum of the H_2O_2 generation rate is shown as the slope of the H_2O_2 amount curve under illumination (Figure 5c, red), which is higher than other recent PEC systems for H_2O_2 production without external bias (Table 1). *J–V* curves of the other cathodes as control groups are compared in Figure S6 (Supporting Information). The *J–t* curve for 300 min electrolysis is plotted in Figure S7 (Supporting Information). The morphology for the electrodes before and after 300 min electrolysis is shown in Figure S8 (Supporting Information).

In terms of electricity generation, the light-driven fuel cell has an open-circuit voltage (V_{oc})of 0.61 V and a short-circuit density (J_{sc}) of 1.09 mA cm^{-2} (Figure 5d), which is consistent with the chopped *J–t* curve. The maximum output power density is 0.194 mW cm^{-2}. The comparison of the performance with other PFCs' is summarized in Table S1 (Supporting Information). The electricity generation capability under light is further confirmed by a simple multimeter measurement (Movie S1, Supporting Information). The generated electricity is sufficient to further brighten a LED light bulb as well (Figure S9, Supporting Information). The LED light demonstration and the multimeter measurement can also be utilized as the sign to determine the cell functioning well or not, which gives a good indication for the simultaneous H_2O_2 evolution without direct detection from the cell.

3. Conclusion

We have successfully designed and implemented a new type of unassisted PEC system. This unassisted PEC system works as a light-driven fuel cell and uses light to convert water and oxygen to a valuable chemical H_2O_2 on photoanode and cathode with simultaneous generation of electricity, i.e., light + $2H_2O$ + O_2 = electricity + $2H_2O_2$. We have optimized this light-driven fuel cell for maximizing the production of H_2O_2. The optimized fuel cell consists of $BiVO_4$ photoanode with

Table 1. Summary of H_2O_2 production rates in recent published photo-electrochemical systems. The production rates (µmol min^{-1} cm^{-2}) are calculated based on the reported electrode geometric area and measurement time provided in each reference. Our system generates H_2O_2 at a higher rate in both unassisted and assisted categories.

Electrode materials		Bias applied	H_2O_2 generation rate	H_2O_2 generation type and electrode geometric area used for calculation	Ref.
Anode	Cathode				
$BiVO_4$	C-cathode	No external bias	0.48	Two side generation from anode + cathode 2 cm^2 for anode/cathode	This work
		1.5 V anode versus cathode	2.42		
		0.32 V versus RHE for cathode (2.4 V anode vs cathode)	7.3		
$WO_3/BiVO_4$	Pt	0.4–1.8 V versus RHE for anode	0.022	One side generation from anode 6.6 cm^2 for anode	[22]
$BiVO_4$	Pt	3.0 V versus Pt mesh for anode, under dark	0.47	One side generation from anode 13.2 cm^2 for anode	[14]
$FeO(OH)/BiVO_4$	Co^{II}(Ch)	No external bias	0.20	One side generation from cathode 2.5 cm^2 for anode	[8b]
WO_3	Co^{II}(Ch)	No external bias	0.13	One side generation from cathode 2.5 cm^2 for anode	[8a]
$WO_3/BiVO_4$	Au	No external bias	0.066	Two side generation from anode + cathode 6.6 cm^2 for anode	[9]
Pt/CB	activated carbon+vapor-grown carbon fiber (AC + VGCF)	0.32 V versus RHE for cathode (rough)	4.8	One side generation from cathode 2 cm^2 for cathode	[20g]

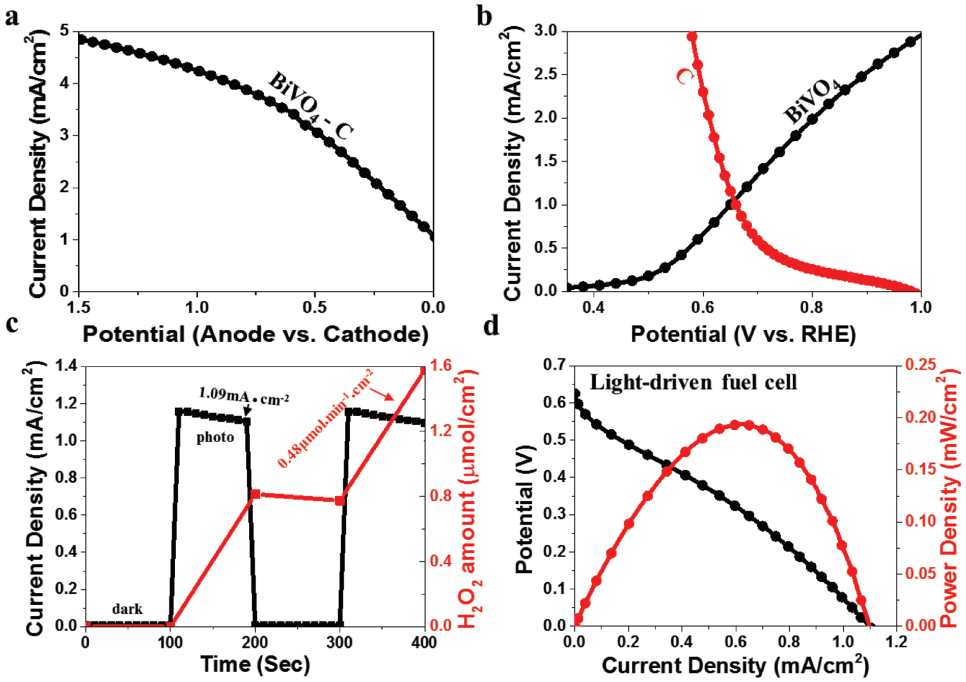

Figure 5. Characterizations for the light-driven fuel cell under 1 sun illumination. The $BiVO_4$ photoanode was in 2 M $KHCO_3$ while the C-cathode was in 1 M Na_2SO_4 with the membrane in between and O_2 purging on both sides. a) The *J–V* curve of $BiVO_4$–C in a two-electrode system, which shows a notable current flow (1.09 mA cm^{-2}) at zero applied bias. b) The *J–V* curve of $BiVO_4$ under illumination intersects with the reversed *J–V* curve of C-cathode at 0.66 V versus RHE, indicating the feasibility of unassisted system. Both *J–V* curves are measured in three-electrode systems (Ag/AgCl as reference electrode and bare FTO as counter electrode). c) The chopped *J–t* curve of $BiVO_4$–C in a two-electrode system without external bias. Clearly, H_2O_2 is spontaneously generated only under illumination. d) The *J–V* curve for the light-driven fuel cell (black) and the calculated power density curve (red). All the tests were conducted in an O_2 saturated electrolyte with a pH around 8.3.

$KHCO_3$ as electrolyte and C-cathode with Na_2SO_4 as electrolyte, with a membrane in between and O_2 purging on both sides. This optimized light-driven fuel cell produces H_2O_2 at a rate of 0.48 μmol min^{-1} cm^{-2}, the highest value compared to other H_2O_2 unassisted production work. It simultaneously yields a maximum output power density of 0.194 mW cm^{-2}, exceeding many other photocatalysis fuel cells for organic decomposition. Importantly, this fuel cell can produce H_2O_2 using tap water, signifying the potential for water disinfection. This light-driven fuel cell can be further improved by using a photocathode part with narrower bandgap than the photoanode to utilize broader range of solar spectrum. We believe that this work represents a new direction, beyond traditional PEC water splitting to produce H_2 and O_2 with/without additional bias, to produce other valuable chemicals and electricity simultaneously. As a next step for this new type of light-driven fuel cells, many studies are needed in the future. Just to name a few here, $BiVO_4$ is toxic and not stable in a wide pH range, so that other environmental friendly and stable photoanodes need to be developed for practical application. Moreover, higher concentration of H_2O_2 tends to dissociate, so H_2O_2 stabilization methods and design of a flow cell system are needed to achieve high concentration of H_2O_2.

4. Experimental Section

Fabrication of Photoanode and Cathode: The photoanode was prepared by spin-coating the $BiVO_4$ precursor on FTO followed by thermal annealing. The $BiVO_4$ precursor solution was a mixture of vanadyl acetylacetonate ($C_{10}H_{14}O_5V$, 98%, Aldrich), and bismuth nitrate hexahydrate ($BiN_3O_9{\cdot}5H_2O$, 99.99%, Aldrich). They were added to a solution of acetylacetone ($C_5H_8O_2$, Aldrich) and acetic acid (CH_3COOH, 99.70%, Fisher) with a ratio 1:0.12. The mixture was sonicated for 10 min, and used within 1 day after preparation. The final molar concentration of Bi was 0.08 M. Before depositing $BiVO_4$, a SnO_2 hole blocking layer was coated on FTO by spin-coating the precursor ($SnCl_2{\cdot}2H_2O$, 50×10^{-3} M, Aldrich, dissolved in isopropyl alcohol, IPA) at 3000 rpm for 30 s followed by annealing at 500 °C for 50 min. After then, the prepared $BiVO_4$ precursor solution (100 μL) was dropped on top with a two-step spin coating process for 5 s at 500 rpm and 30 s at 3000 rpm. After drying at 100 °C for 10 min, the samples were then annealed at 300, 400, and 500 °C for 5 min, sequentially. The above coating and annealing processes for $BiVO_4$ were repeated for 15 cycles, followed by 500 °C annealing for 2 h in the final stage.

The C-cathode was prepared by drop casting CMK-3 on carbon paper. First, the ordered mesoporous carbon powder (4 mg) CMK-3 was dispersed in 2 mL ethanol, along with H_2O (0.4 mL) and Nafion solution (50 μL, Aldrich, 5 wt%). The obtained suspension was sonicated for 30 min. Then, the suspension was drop casted to the Sigracet Graphite carbon paper (Ion Power, with hydrophobic gas diffusion layer on the back side) as an air-breathing cathode followed by drying at ambient conditions. The CMK-3 loading was ≈140 μg cm^{-2}.

Characterization of Photo-Electrochemical Performance: For the electrochemical tests, the experiments were carried out by using a potentiostat Gamry Interface 1000 Potentiostat (Gamry Instruments Inc.), with Ag/AgCl electrode used as the reference electrode in a three-electrode system. Silver paste was used to make metal contact for each sample. The measurements under illumination were obtained under 1 sun and AM 1.5G using a solar simulator for irradiation.

$KHCO_3$ (2 M) was used as the electrolyte for the anode part, and Na_2SO_4 (1 M) was used as the electrolyte for the cathode part. A

membrane (Nafion perfluorinated membrane, Aldrich) was used to separate the anode part and the cathode part, which allowed the exchange of protons and oxygen[27] while blocked the diffusion of HCO_3^- and H_2O_2. In this way, the negative effect of HCO_3^- for the cathode part could be inhibited and concentration of H_2O_2 at two half-cells could be detected separately. The bottom half of the cell was immersed in the ice water for the measurements that over 30 min. The instantaneous concentration of H_2O_2 was measured using standard H_2O_2 test strips (Indigo Instruments) periodically, which yielded the H_2O_2 concentration as a function of time, further combined with the red, green, blue (RGB) analysis (Supplementary Note S1.6 and Figure S10, Supporting Information). For higher concentration, the amount of H_2O_2 was further confirmed by titration using potassium permanganate ($KMnO_4$, urther confirmed, with the sulfuric acid (H_2SO_4, Acros Organics) used as the H^+ source. The permanganate ion has a dark purple color and the color disappears during titration due to the following equation

$$2MnO_4^- + 5H_2O_2 + 6H^+ \rightarrow 2Mn^{2+} + 5O_2 + 8H_2O \quad \text{(R10)}$$

The Faradaic efficiency for H_2O_2 production (%) is defined as

$$FE = \frac{\text{Amount of } H_2O_2\,(\text{mol})}{\text{Total amout of charge passed}/2\,(\text{mol})} \times 100\% \quad \text{(R11)}$$

Gas chromatography (GC) analysis was carried out using Ar as the carrier gas. The PEC cell was sealed with an inset of Ar, for which the gas flow rate was controlled by a mass flow controller (MFC). The PEC cell had another outlet, which was connected to a GC for gas composition measurement. In between, the evolved gas from the PEC cell passed through a desiccator to remove the water vapor. The sample gas was measured every 4 min and the amount of evolved H_2/O_2 was integrated with respect to the reaction time. The GC was calibrated by the O_2 and H_2 gases with standard concentrations.

Supporting Information

Supporting Information is available from the Wiley Online Library or from the author.

Acknowledgements

X.S. and Y.Z. contributed equally to this work. The authors gratefully acknowledge support from the U.S. Department of Energy, Office of Sciences, Office of Basic Energy Sciences, to the SUNCAT Center for Interface Science and Catalysis. The authors also acknowledge the great technical assistance and suggestions on this work from Jens K. Norskov, Professor of Chemical Engineering and Photon Science, Stanford University.

Conflict of Interest

The authors declare no conflict of interest.

Keywords

light-driven fuel cells, oxygen reduction, power density, two-electron pathway, water oxidation

Received: April 17, 2018
Revised: May 8, 2018
Published online: June 21, 2018

[1] A. Fujishima, K. Honda, *Nature* **1972**, *238*, 37.
[2] a) O. Monfort, L.-C. Pop, S. Sfaelou, T. Plecenik, T. Roch, V. Dracopoulos, E. Stathatos, G. Plesch, P. Lianos, *Chem. Eng. J.* **2015**, *286*, 91; b) O. Khaselev, J. A. Turner, *Science* **1998**, *280*, 425.
[3] a) Q. Chen, J. Li, X. Li, K. Huang, B. Zhou, W. Cai, W. Shangguan, *Environ. Sci. Technol.* **2012**, *46*, 11451; b) J. Li, J. Li, Q. Chen, J. Bai, B. Zhou, *J. Hazard. Mater.* **2013**, *262*, 304; c) M. Antoniadou, P. Lianos, *Photochem. Photobiol. Sci.* **2011**, *10*, 431; d) D. Wang, Y. Li, G. L. Puma, P. Lianos, C. Wang, P. Wang, *J. Hazard. Mater.* **2017**, *323*, 681.
[4] a) M. Sui, Y. Dong, H. You, *RSC Adv.* **2015**, *5*, 94184; b) J. Bai, R. Wang, Y. Li, Y. Tang, Q. Zeng, L. Xia, X. Li, J. Li, C. Li, B. Zhou, *J. Hazard. Mater.* **2016**, *311*, 51; c) Q. Chen, J. Li, X. Li, K. Huang, B. Zhou, W. Shangguan, *ChemSusChem* **2013**, *6*, 1276.
[5] a) K. Sivula, R. Van De Krol, *Nat. Rev. Mater.* **2016**, *1*, 15010; b) M. Antoniadou, P. Lianos, *Appl. Catal., B* **2010**, *99*, 307.
[6] M. Kaneko, J. Nemoto, H. Ueno, N. Gokan, K. Ohnuki, M. Horikawa, R. Saito, T. Shibata, *Electrochem. Commun.* **2006**, *8*, 336.
[7] a) K. Li, H. Zhang, Y. Tang, D. Ying, Y. Xu, Y. Wang, J. Jia, *Appl. Catal., B* **2015**, *164*, 82; b) C. Hu, D. Kelm, M. Schreiner, T. Wollborn, L. Mädler, W. Y. Teoh, *ChemSusChem* **2015**, *8*, 4005; c) P. Lianos, *Appl. Catal., B* **2017**, *210*, 235.
[8] a) K. Mase, M. Yoneda, Y. Yamada, S. Fukuzumi, *Nat. Commun.* **2016**, *7*, 11470; b) K. Mase, M. Yoneda, Y. Yamada, S. Fukuzumi, *ACS Energy Lett.* **2016**, *1*, 913.
[9] K. Fuku, Y. Miyase, Y. Miseki, T. Funaki, T. Gunji, K. Sayama, *Chem. - Asian J.* **2017**, *12*, 1111.
[10] A. J. Bard, R. Parsons, J. Jordan, *Standard Potentials in Aqueous Solution*, Vol. *6*, CRC Press, Boca Raton, FL **1985**.
[11] a) S. J. Hong, S. Lee, J. S. Jang, J. S. Lee, *Energy Environ. Sci.* **2011**, *4*, 1781; b) A. J. Rettie, H. C. Lee, L. G. Marshall, J.-F. Lin, C. Capan, J. Lindemuth, J. S. McCloy, J. Zhou, A. J. Bard, C. B. Mullins, *J. Am. Chem. Soc.* **2013**, *135*, 11389.
[12] S. Siahrostami, G.-L. Li, V. Viswanathan, J. K. Nørskov, *J. Phys. Chem. Lett.* **2017**, *8*, 1157.
[13] A. Izgorodin, E. Izgorodina, D. R. MacFarlane, *Energy Environ. Sci.* **2012**, *5*, 9496.
[14] K. Fuku, Y. Miyase, Y. Miseki, T. Gunji, K. Sayama, *ChemistrySelect* **2016**, *1*, 5721.
[15] X. Shi, S. Siahrostami, G.-L. Li, Y. Zhang, P. Chakthranont, F. Studt, T. F. Jaramillo, X. Zheng, J. K. Nørskov, *Nat. Commun.* **2017**, *8*, 701.
[16] V. Viswanathan, H. A. Hansen, J. K. Nørskov, *J. Phys. Chem. Lett.* **2015**, *6*, 4224.
[17] a) S. Siahrostami, A. Verdaguer-Casadevall, M. Karamad, D. Deiana, P. Malacrida, B. Wickman, M. Escudero-Escribano, E. A. Paoli, R. Frydendal, T. W. Hansen, I. Chorkendorff, I. E. L. Stephens, J. Rossmeisl, *Nat. Mater.* **2013**, *12*, 1137; b) A. Verdaguer-Casadevall, D. Deiana, M. Karamad, S. Siahrostami, P. Malacrida, T. W. Hansen, J. Rossmeisl, I. Chorkendorff, I. E. Stephens, *Nano Lett.* **2014**, *14*, 1603.
[18] J. S. Jirkovský, I. Panas, E. Ahlberg, M. Halasa, S. Romani, D. J. Schiffrin, *J. Am. Chem. Soc.* **2011**, *133*, 19432.
[19] a) S. Siahrostami, M. E. Björketun, P. Strasser, J. Greeley, J. Rossmeisl, *Phys. Chem. Chem. Phys.* **2013**, *15*, 9326; b) M. Campos, W. Siriwatcharapiboon, R. J. Potter, S. L. Horswell, *Catal. Today* **2013**, *202*, 135.
[20] a) E. Peralta, R. Natividad, G. Roa, R. Marin, R. Romero, T. Pavon, *Sustainable Environ. Res.* **2013**, *23*, 259; b) R. A. Sidik, A. B. Anderson, N. P. Subramanian, S. P. Kumaraguru, B. N. Popov, *J. Phys. Chem. B* **2006**, *110*, 1787; c) Y. Lu, M. Wang, C. Yuan, J. Zhao, J. Yu, *Int. J. Electrochem. Sci.* **2015**, *10*, 2825; d) T.-P. Fellinger, F. Hasché, P. Strasser, M. Antonietti, *J. Am. Chem. Soc.* **2012**, *134*, 4072; e) J. Park, Y. Nabae, T. Hayakawa, M.-a. Kakimoto, *ACS Catal.* **2014**, *4*, 3749; f) Y.-H. Lee, F. Li, K.-H. Chang, C.-C. Hu, T. Ohsaka, *Appl. Catal., B* **2012**, *126*, 208; g) I. Yamanaka, T. Murayama, *Angew. Chem., Int. Ed.* **2008**, *47*, 1900.

[21] Z. Chen, S. Chen, S. Siahrostami, P. Chakthranont, C. Hahn, D. Nordlund, S. Dimosthenis, J. K. Nørskov, Z. Bao, T. F. Jaramillo, *React. Chem. Eng.* **2017**, *2*, 239.
[22] K. Fuku, K. Sayama, *Chem. Commun.* **2016**, *52*, 5406.
[23] a) D. E. Richardson, H. Yao, K. M. Frank, D. A. Bennett, *J. Am. Chem. Soc.* **2000**, *122*, 1729; b) J. Flangan, D. P. Jones, W. P. Griffith, A. C. Skapski, A. P. West, *J. Chem. Soc., Chem. Commun.* **1986**, 20; c) A. Adam, M. Mehta, *Angew. Chem., Int. Ed.* **1998**, *37*, 1387.
[24] M. Rahimnejad, G. Bakeri, M. Ghasemi, A. Zirepour, *Polym. Adv. Technol.* **2014**, *25*, 1426.
[25] a) J. M. Harvey, G. M. Clark, C. K. Osborne, D. C. Allred, *J. Clin. Oncol.* **1999**, *17*, 1474; b) C. Li, S. Ziesmer, O. Lazcano-Villareal, *J. Histochem. Cytochem.* **1987**, *35*, 1457.
[26] D. Ing, O. Zajic, presented at Fourth Int. Water Technology Conf., Alexandria, Egypt, March **1999**.
[27] V. A. Sethuraman, S. Khan, J. S. Jur, A. T. Haug, J. W. Weidner, *Electrochim. Acta* **2009**, *54*, 6850.